SYNTHESIS AND CHARACTERIZATION OF COBALT, COPPER AND ZINC SUBSTITUTED BIOGLASSES OBTAINED BY THE SOL-GEL METHOD

Ana-Maria-Raluca MUȘAT[1], Gabriela-Olimpia ISOPENCU[2], Cristina BUSUIOC[3]

The purpose of the work is to obtain innovative bioglasses suitable for biomedical applications. The sol-gel method was used to synthesize bioglasses with four different compositions, where CaO was partially substituted with 1 mol% CoO, and 5 mol% CuO or ZnO, respectively. The bioglass samples were characterized by thermal analysis (TA), X-ray diffraction (XRD), Fourier-transform infrared spectroscopy (FTIR), scanning electron microscopy (SEM), and energy-dispersive X-ray spectroscopy (EDX). The thermal analysis revealed three main mass loss stages a total weight loss of approximately 46 %, confirming that the chosen calcination temperature of 700 °C is appropriate. XRD indicated an insignificant crystallization tendency for the substituted bioglasses, with broad halos around 2θ value of 25-35 °, validating their amorphous nature. FTIR showed the structural evolution of bioglass compositions during processing, highlighting the removal of residual nitrates and organic groups and the formation of Si–O–Si and Si–O–Ca bonds above 600 °C. SEM illustrated the morphological differences induced by the substituents, with BGCu showing a more compact and homogenous microstructure. EDX confirmed the incorporation of Co, Cu and Zn elements in the bioglass matrices, according with the nominal compositions. Antibacterial activity was also assessed using the disk diffusion method against Bacillus subtilis and Escherichia coli, with considerable inhibition zones especially for BGCu, demonstrating the enhanced antimicrobial potential of substituted bioglasses in the medical field.

Keywords: bioglass, substitution, sol-gel, antibacterial activity

1. Introduction

The discovery of bioglass by Professor Hench in the 1970s revolutionized the field of biomaterials, marking the beginning of a new generation of bioactive materials for clinical applications. Unlike the early generations of biomaterials,

[1] PhD Student, Department of Science and Engineering of Oxide Materials and Nanomaterials, National University of Science and Technology POLITEHNICA Bucharest, Romania, e-mail: ana_maria.musat@stud.chimie.upb.ro

[2] Associate Professor, Department of Chemical and Biochemical Engineering, National University of Science and Technology POLITEHNICA Bucharest, Romania, e-mail: gabriela.isopencu@upb.ro

[3] Full Professor, Department of Science and Engineering of Oxide Materials and Nanomaterials, National University of Science and Technology POLITEHNICA Bucharest, Romania, e-mail: cristina.busuioc@upb.ro

which focused on minimizing adverse tissue reactions, bioglasses were designed to foster active interactions between the material and tissue, thereby promoting tissue regeneration and integration. Bioglass is characterized by the formation of a hydroxycarbonate apatite (HCA) layer at the interface with the biological environment, which is chemically and structurally equivalent to the mineral phase of bone [1]. The versatility of bioglasses in biomedical applications, including their use as implant coatings [2] and regenerative materials, has been extensively studied, emphasizing their bioactivity, osseointegration and antimicrobial properties [3, 4]. For instance, 45S5 bioglass coatings have demonstrated efficacy in inhibiting bacterial growth, including *Staphylococcus aureus* and *Escherichia coli*, through mechanisms such as increasing the local pH and releasing bioactive ions, which disrupt bacterial biofilms [5, 6]. Furthermore, noble metal-containing bioglasses, including those with silver and gold nanoparticles, have shown significant promise in bone tissue engineering, enhancing both osteogenic and antibacterial outcomes, with promising results *in vitro* for promoting cell proliferation and apatite formation [7, 8]. The integration of gold-silver nanocages into bioglasses was shown to enhance the antibacterial properties through unique mechanisms of biofilm disruption [9]. Silver-substituted bioglasses exhibit not only antibacterial activity, but also osteogenic potential, making them suitable for advanced implant technologies [10]. These findings underscore the potential of bioglass coatings, both simple and substituted, in advancing implant technology and preventing post-surgical complications [11, 12].

The composition of bioglass is adapted to facilitate the formation of this interface, and the addition of metal oxides, such as CoO, CuO, and ZnO, was shown to enhance its bioactive properties and suitability for both hard and soft tissue applications.

Baino *et al.* [13] highlighted cobalt as a promising substituent due to its dual role in promoting osteogenesis and angiogenesis. Cobalt-substituted bioglass releases osteoinductive ions, creating microenvironments favourable to bone growth and vascularization. Studies indicate that cobalt allows for a slower dissolution rate and controlled ion release, which is particularly advantageous for scaffolds requiring prolonged bioactivity. Solanki *et al.* [14] further emphasized its ability to stimulate blood vessel formation and enhance regenerative conditions, making it suitable for both bone repair and wound healing with confirmed formation of HCA and antibacterial effects in samarium-doped systems [15]. Additionally, structural characterization studies performed by Jones *et al.* [16] revealed the hypoxia-mimicking effects of cobalt-substituted bioactive glasses, providing insights into their role in angiogenesis and cellular response. However, higher concentrations of cobalt can lead to toxicity, several studies showing reduced cell viability at levels above 10 ppm. Therefore, cobalt must be

used in controlled amounts to balance its therapeutic benefits and minimize potential cytotoxic effects [14, 16].

Hammami *et al.* [17] reported that CuO-substituted 45S5 bioglass significantly enhances antibacterial properties and bioactivity, even at low concentrations, such as 0.5 mol%. Copper ions play a vital role in collagen synthesis, wound healing, and vascularization during bone repair. Furthermore, Türe [18] demonstrated that copper-substituted bioglass supports osteointegration and exhibits notable antioxidant and pro-angiogenic properties. Additionally, copper-substituted bioglasses showed promising results in dental applications, combining their regenerative properties with effective antimicrobial activity [17]. These findings emphasize the potential of copper-containing bioglass for implant coatings, particularly in applications requiring enhanced antibacterial activity and improved vascularization.

Zinc-substituted bioglasses synthesized via the sol-gel method demonstrated significant biological properties, particularly in promoting bone tissue engineering and antimicrobial effects [19, 20]. The addition of ZnO was shown to enhance bioactivity [21] and osteoconductivity, with controlled degradation and ion release playing a crucial role in its performance [22, 23]. Babu *et al.* [24] demonstrated that ZnO-substituted bioglass promotes bone growth and enhances antibacterial properties. Specifically, the incorporation of ZnO enables controlled degradation of the glass in synthetic body fluid, with optimal antibacterial activity against *E. coli* and *S. aureus* observed at 8 mol% ZnO. Additionally, Nescakova *et al.* [25] reported that ZnO incorporation supports osteoblast differentiation and protein adsorption, creating favourable conditions for cellular attachment and proliferation. Structural analysis of ZnO-substituted bioglasses using FTIR and XRD [26] confirmed the reinforcement of Si–O and P–O bonds, contributing to enhanced thermal stability and resistance to crystallization [22]. However, higher levels of zinc release, exceeding the therapeutic limits, may lead to cytotoxic effects, as observed in studies indicating reduced cell viability at elevated ZnO concentrations. These findings underscore the importance of optimizing zinc content in bioglass to balance bioactivity and biocompatibility, making ZnO-containing bioglass a suitable candidate for resorbable implants.

Modern synthesis methods like sol-gel enable precise control over the composition and ion release of bioglasses, broadening their applications in medical implants and tissue engineering, and facilitate integration into coating processes such as pulsed laser deposition and spin coating [8]. In this study, the structural and morphological characterization of both unsubstituted and substituted bioglasses was performed to evaluate their suitability for thin-film deposition applications [27]. Advanced characterization techniques revealed the structural stability of substituted bioglasses, with particular emphasis on their

amorphous nature and robust Si–O bonding [14, 24, 28]. These findings align with previous reports on sol-gel-derived bioactive glasses exhibiting high thermal stability and minimal crystallization tendency.

2. Experimental procedure

In the laboratory, were prepared powders of both unsubstituted and substituted bioglass with cobalt, copper and zinc, using the following compositions (mol%):

- 60 % SiO_2 – 4 % P_2O_5 – 36 % CaO (BG);
- 60 % SiO_2 – 4 % P_2O_5 – 35 % CaO – 1 % CoO (BGCo).
- 60 % SiO_2 – 4 % P_2O_5 – 31 % CaO – 5 % CuO (BGCu);
- 60 % SiO_2 – 4 % P_2O_5 – 31 % CaO – 5 % ZnO (BGZn);

For cobalt, a lower concentration (1 mol%) was selected due to the demonstrated toxicity of cobalt in higher amounts, ensuring that the substituted bioglass remains biocompatible.

The preparation process began with the calculation of precise quantities for each reagent required to achieve the desired compositions. Tetraethyl orthosilicate ($Si(OC_2H_5)_4$, TEOS) was used as the silicon source, while triethyl phosphate ($(C_2H_5)_3PO_4$, TEP) and calcium nitrate tetrahydrate ($Ca(NO_3)_2{\cdot}4H_2O$) served as sources for phosphorus and calcium, respectively. The substituted bioglasses incorporated additional precursors specific to each element: cobalt nitrate hexahydrate ($Co(NO_3)_2{\cdot}6H_2O$), copper nitrate trihydrate ($Cu(NO_3)_2{\cdot}3H_2O$), and zinc nitrate hexahydrate ($Zn(NO_3)_2{\cdot}6H_2O$). These precursors were carefully selected for their high solubility and compatibility with the sol-gel synthesis process.

The synthesis of all the bioglass samples was performed using the sol-gel method, as outlined in Fig. 1. This method involves the sequential preparation and mixing of precursors, followed by thermal treatments to achieve the desired bioglass composition and structure.

TEOS was dissolved in ethanol, while TEP and the nitrates (used as precursors for Ca, Co, Cu, and Zn) were dissolved in distilled water. During the mixing of TEOS, nitric acid was added to adjust the *p*H to 1-2, a critical step for the hydrolysis and condensation reactions that form the silica network. The individual components were mixed in the following order: nitrates, TEP, and finally TEOS. This mixture was then left to homogenize further under magnetic stirring for 1 h at room temperature. The homogeneous solution was transferred to an oven at 70 °C for a minimum of 48 h to form a gel. After gelation and aging, the resulting material was left to dry for an additional 48 h at the same temperature, producing a fully dried gel. The dried gel was then calcined at 600 °C for 48 h to remove all residues and ensure the formation of the glass structure.

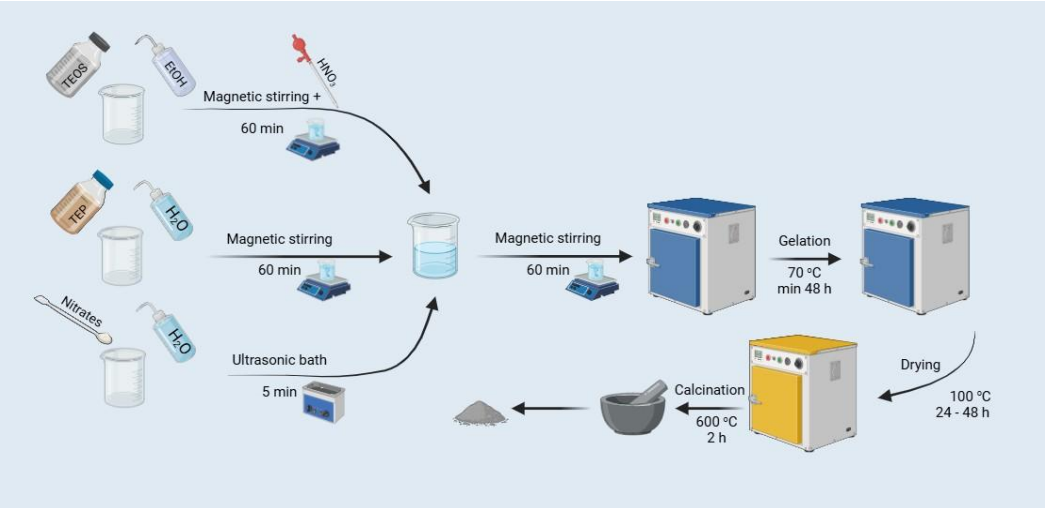

Fig. 1. Synthesis of bioglass using the sol-gel method.

The resulting material was a coarse powder of calcined bioglass. To finalize the preparation, the calcined powder was ground into a fine powder using a mortar and pestle. The stepwise synthesis process is further illustrated in Fig. 2, which presents images of the bioglass powder synthesis stages captured during the laboratory procedures:

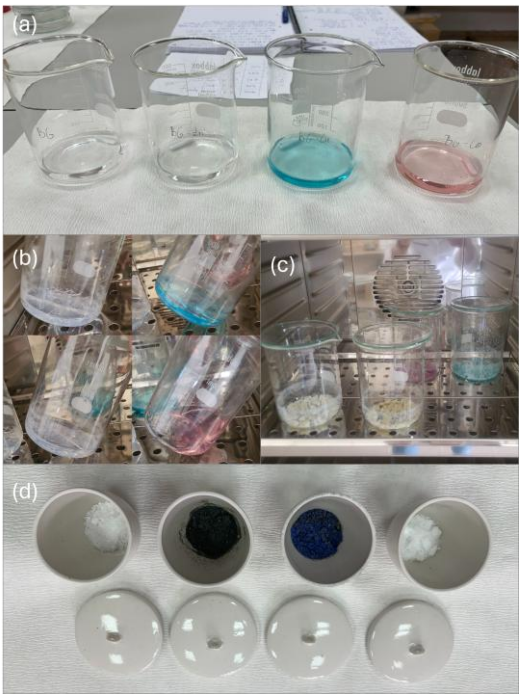

Fig. 2. Stages of bioglass powder synthesis: (a) initial solutions, (b) gels formation, (c) dried gels, and (d) calcined powders for unsubstituted and Co-, Cu-, and Zn-substituted bioglasses.

The thermal analysis was carried out using a Netzsch STA 449 F3 Jupiter equipment. The dried sample was placed in an alumina crucible and heated from 20 to 900 °C at a constant rate of 10 °C/min, in air. The X-Ray Diffraction (XRD) was performed with a Shimadzu XRD 6000 diffractometer equipped with a Cu X-ray tub operating at 40 kV and 30 mA. The scan was carried out in continuous mode over a 2θ range of 10 to 70 °, with a step size of 0.02 °, at a scan speed of 2 °/min and a preset time of 0.6 s. The Fourier Transform Infrared Spectroscopy was conducted in the Attenuated Total Reflectance (ATR) mode on a Thermo Scientific Nicolet iS50 spectrophotometer. The wavenumber was ranged between 400 and 4000 cm^{-1}, with a 4 cm^{-1} resolution and 32 scans/sample. Scanning Electron Microscopy (SEM) coupled with Energy-Dispersive X-Ray Spectroscopy (EDX) were achieved employing a FEI Quanta Inspect F50 microscope operated at 30 kV accelerating voltage and equipped with an EDX probe. The working distance was set at 10 mm, and the samples were previously gold coated by DC magnetron sputtering for 60 s.

3. Results and discussion

Thermal analysis (TA) was performed to assess the thermal stability and decomposition behaviour of the obtained unsubstituted gel (Fig. 3a). The mass loss curve indicated a significant reduction in mass, approximately 47 %, occurring up to 600 °C. This observation was supported by the derivative thermogravimetry (DTG) and differential scanning calorimetry (DSC) curves, which revealed three large stages of mass loss and several thermal effects: (i) around 200 °C, the evaporation of residual water associated with an endothermic process; (ii) at approximately 400 °C, the first stage of nitrates decomposition corresponding to an area of complex thermal effects since secondary processes could occur, like organic components burning or incipient crystallization; (iii) beyond 500 °C, the total elimination of nitrates attributed to an endothermic effect. These findings confirm that a calcination temperature of 600 °C is optimal, ensuring the removal of volatile components while preserving the structural integrity of the bioglass.

The X-ray diffraction (XRD) analysis was employed to evaluate the structural properties of the bioglasses (Fig. 3b). The XRD patterns of all samples displayed a broad band between 15 and 35 °, characteristic of glassy materials. Notably, the calcination temperature of 600 °C maintained the amorphous structure of the basic composition, with no significant crystallization detected. However, the substituted bioglasses containing Co, Cu, and Zn exhibited a slight tendency toward crystallization, suggesting potential interactions between the additional ions and the glass network. When correlating with the thermal analysis, the absence of diffraction peaks after thermally treating at 600 °C aligns with the removal of unwanted components below this temperature, as observed in the TA

data. The slight crystallization tendency in substituted samples may arise from localized structural rearrangements occurring during calcination [29]. Ion substitution has been shown to influence crystallization behavior by modifying the sintering window and promoting rearrangements within the glass network, which can act as nucleation sites for crystalline phase formation. As discussed by Peitl et al., crystallization does not necessarily inhibit bioactivity but can slow down hydroxyapatite formation, affecting the material's biological response in vivo [29].

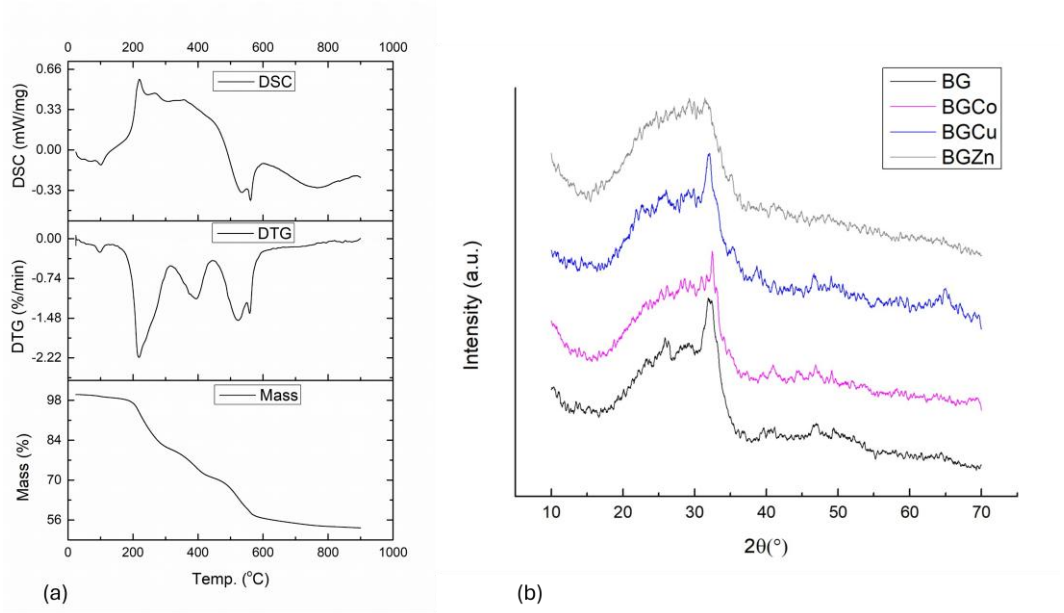

Fig. 3. (a) Thermal analysis and (b) XRD patterns of bioglasses calcined at 600 °C.

The Fourier-transform infrared (FTIR) spectra of the bioglass samples provide insights into their structural evolution during processing. Fig. 4a illustrates the spectrum of the gels dried at 100 °C, which reveals several characteristic vibrational bands. The broad band around 3,500 cm^{-1} corresponds to hydroxyl (OH^-) groups, indicating the presence of residual water and hydrogen-bonded species. The peaks near 1,380 and 1,450 cm^{-1} are associated with nitrate (NO_3^-) groups, likely originating from precursors used during synthesis, while the bands at approximately 1,000 and 1,100 cm^{-1} are attributed to silicate (Si–O) and phosphate (P–O) bonds, practically the units on which the glass network is built. Additionally, the bands around 870 cm^{-1} suggest the presence of carbonate (CO_3^{2-}) impurities caused by reaction with carbon dioxide from air. These features indicate an intermediate stage of bioglass formation, where residual by-products and incomplete reactions are still present.

After calcination at 600 °C, the FTIR spectra demonstrates significant changes (Fig. 4b). The disappearance of the broad hydroxyl band confirms the

removal of residual water and OH^- groups, while the elimination of nitrate and carbonate peaks indicates the decomposition of precursors and impurities during the heat treatment. The remaining vibrational bands are dominated by those associated with silicate (Si–O) and phosphate (P–O) bonds, reflecting the characteristic network structure of bioglass. The most intense Si–O band observed around 1040 cm^{-1} is assigned to the asymmetric stretching (Si–O_as), while the band near 460 cm^{-1} corresponds to the bending vibrations of the Si–O bonds (Si–O_b), confirming the polymerization of the silicate network after calcination. The absence of impurity-related bands and the sharpening of the silicate and phosphate peaks suggest a more stable and homogeneous structure in the calcined powders.

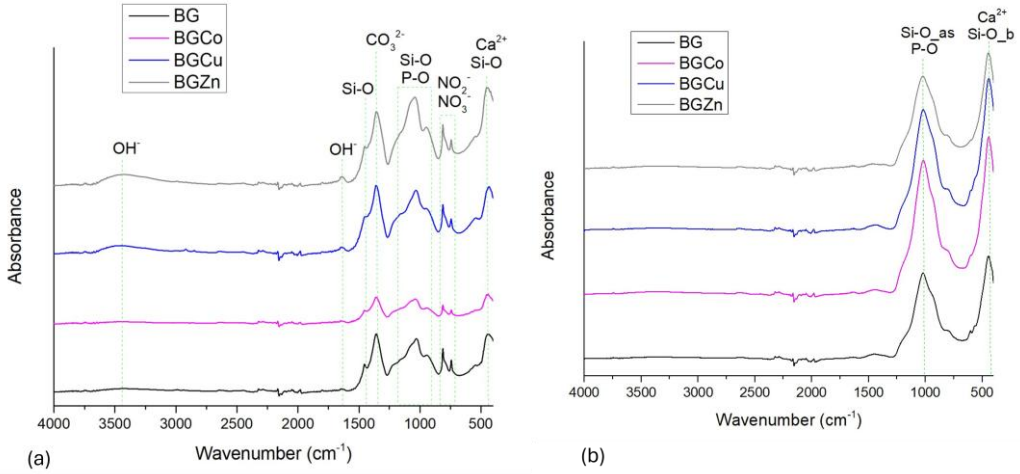

Fig. 4. FTIR spectra of: (a) gels dried at 100 °C and (b) powders calcined at 600 °C. The Si–O bands are labelled as: Si–O_as for asymmetric stretching mode and Si–O_b for bending mode.

The comparison between the FTIR spectra for the dried gels (Fig. 4a) and the calcined powders (Fig. 4b) highlights the structural evolution of bioglass during the thermal treatment. While the dried gel retains a complex spectrum indicative of residues and an intermediate structure, the calcined powder presents a purer profile dominated by the intrinsic bonds of bioglass. This confirms the successful removal of impurities and the stabilization of the bioglass network through calcination.

The scanning electron microscopy (SEM) images at a magnification of 20,000× (Fig. 5) and 200,000× (Fig. 6) illustrate the morphological differences between the bioglass powders. At lower magnification (Fig. 5), BG (Fig. 5a) shows large fragments with irregular edges, characteristic for unsubstituted bioglass. BGCo (Fig. 5b) displays similar large fragments, but with more pronounced densification and the presence of filament-like plates, suggesting that cobalt substitution may induce material reorganization. BGCu (Fig. 5c) exhibits

smoother surfaces and a more tightly packed microstructure, while BGZn (Fig. 5d) has large fragments with irregular edges but appears more uniform and compact compared to BGCu.

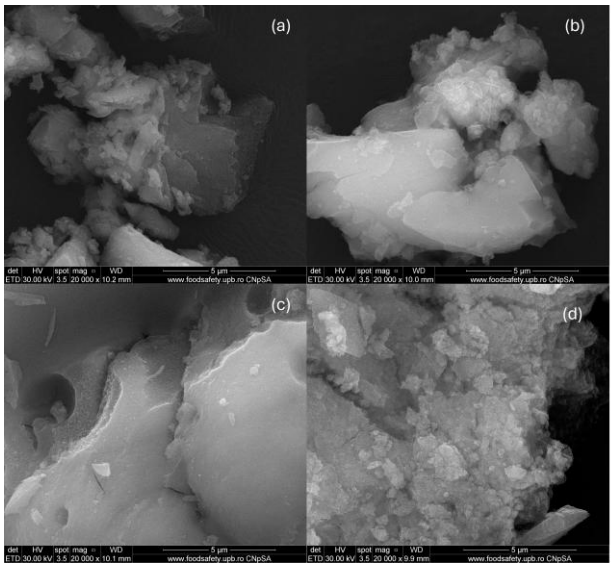

Fig. 5. SEM images of bioglass powders at 20,000× magnification:
(a) BG, (b) BGCo, (c) BGCu, and (d) BGZn.

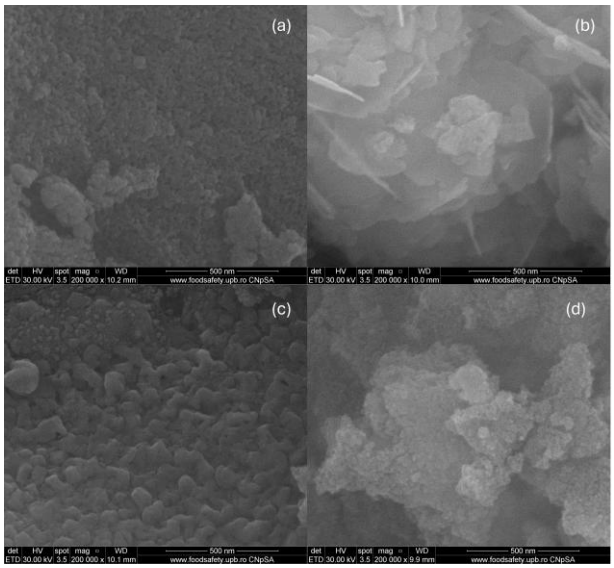

Fig. 6. SEM images of bioglass powders at 200,000× magnification:
(a) BG, (b) BGCo, (c) BGCu, and (d) BGZn.

At higher magnification (Fig. 6), the differences in microstructure become more apparent. BG (Fig. 6a) presents an aggregated morphology with uniformly

distributed fine particles (100–300 nm), consistent with the amorphous nature of the unsubstituted bioglass. BGCo (Fig. 6b) shows densely packed particles and filamentous entities, indicating the influence of cobalt on densification and material organization. BGCu (Fig. 6c) is characterized by quasi-spherical particles (300–500 nm) and a more closely aggregated microstructure, suggesting that copper significantly promotes particle growth. In contrast, BGZn (Fig. 6d) demonstrates a densified and uniform morphology, with particle sizes ranging from 250 to 450 nm, providing a balance between growth and structural stability.

The Energy-dispersive X-ray (EDX) spectra confirms the elemental composition of the bioglass powders, revealing the incorporation of cobalt, copper, and zinc into their respective matrices (Fig. 7). The unsubstituted bioglass (BG) displays the primary elements characteristic of bioglass (Si, Ca, P), as expected. In the modified samples, the intensity of the substituent peaks varies, with copper and zinc showing higher intensities than cobalt, indicating quantitative incorporation into the glass network. Due to the absence of elemental mapping, no conclusions can be drawn regarding the spatial distribution of the dopants. The filament-like entities observed in Fig. 6b may suggest local compositional/structural variations in BGCo, while the more homogenous morphology of BGCu and BGZn (Figs. 6c and 6d) may reflect a more uniform microstructural organization.

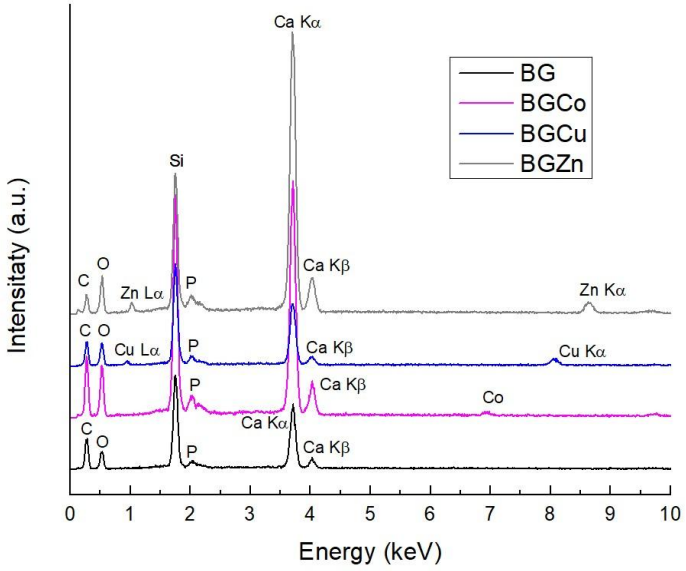

Fig. 7. EDX spectra of bioglasses calcined at 600 °C.

The combination of SEM and EDX provide insights into both the morphology and elemental presence in the substituted bioglasses. Cobalt appears to promote densification and filamentous entities, as observed in the case of

BGCo. Copper enhances particle growth and porosity, as seen for BGCu, while zinc provides a balance between particle growth and structural stability, as evident for BGZn. These findings underscore the versatility of substituted bioglasses in tailoring material properties for specific applications.

The morphological characteristics observed in the present study align with the findings reported by Tulyaganov *et al.* [30], who investigated the structural features of classical 45S5 and CaO-rich bioglass powders. Their sample BG Ca/Mix presents similarities to BGCu and BGZn in our work, exhibiting large particles with increased roughness and a more tightly packed microstructure. This behavior is consistent with the influence of substitutes such as copper and zinc, which enhance particle growth and contribute to surface irregularity. However, the presence of potassium in BG Ca/Mix differentiates its reactivity, contributing to enhanced thermal properties compared to the samples in this study. Conversely, BG 45S5 [30] retains a finer and more amorphous structure, closely resembling the unsubstituted and cobalt-substituted bioglass powders from this work. Unlike BGCu and BGZn, BG 45S5 does not exhibit significant particle growth, highlighting the impact of additions on structural reorganization and morphology.

These findings underline the versatility of substituted bioglasses in tailoring structural and chemical properties for specific biomedical applications, with copper and zinc showing the most significant effects on particle growth and morphological evolution, while cobalt primarily influences densification and filament-like structures. Since EDX confirmed the presence of substituent elements in all compositions, further studies including elemental mapping are needed to fully assess their spatial distribution within the bioglass matrix.

The antimicrobial properties of bioactive glasses have been widely investigated, with multiple studies demonstrating their effectiveness against bacterial biofilms and their potential to address antimicrobial resistance. Previous research highlights the superior antibacterial and anti-biofilm activity of substituted bioactive glasses, particularly those incorporating silver and ceria, which disrupt biofilm formation and enhance antibacterial activity [5, 31, 32]. Furthermore, early-stage bacterial adhesion on bioglass surfaces has been explored using atomic force microscopy, providing insights into their antibacterial mechanisms, including ion release and surface interactions [31]. These findings emphasize the role of bioglass compositions and substitutes in modifying antibacterial properties and inhibiting bacterial colonization.

In this study, the antimicrobial activity of bioglass powder samples was preliminarily evaluated against Gram-negative *Escherichia coli* (DH5K strain) and Gram-positive *Bacillus subtilis spizizenii nakamura* (ATCC 6633), cultured on Luria Bertani (LB) agar. LB is a highly referenced, nutrient-rich medium commonly used for microbial growth, particularly for *E. coli* cultures. The results

revealed significant differences in activity among the substituted bioglasses, highlighting the impact of metallic ion substitution on bacterial inhibition.

For *B. subtilis*, BG-Cu exhibited the highest antimicrobial activity, with a clear inhibition zone (IZ) exceeding 10 mm and a hollow zone (HZ) greater than 15 mm, followed by BG-Zn with a moderate IZ over 6 mm, and BG-Co, which showed limited activity (IZ ~1 mm, HZ >6 mm). In the case of *E. coli*, BG-Cu again demonstrated superior performance (IZ >10 mm, HZ >20 mm), while BG-Co exhibited moderate activity (no clear IZ, HZ ~8 mm), and BG-Zn showed minimal activity (no IZ, HZ <6 mm). Fig. 8 illustrates the variations in antimicrobial activity observed for *B. subtilis* and *E. coli*, respectively, highlighting the superior performance of BG-Cu compared to BG-Zn and BG-Co.

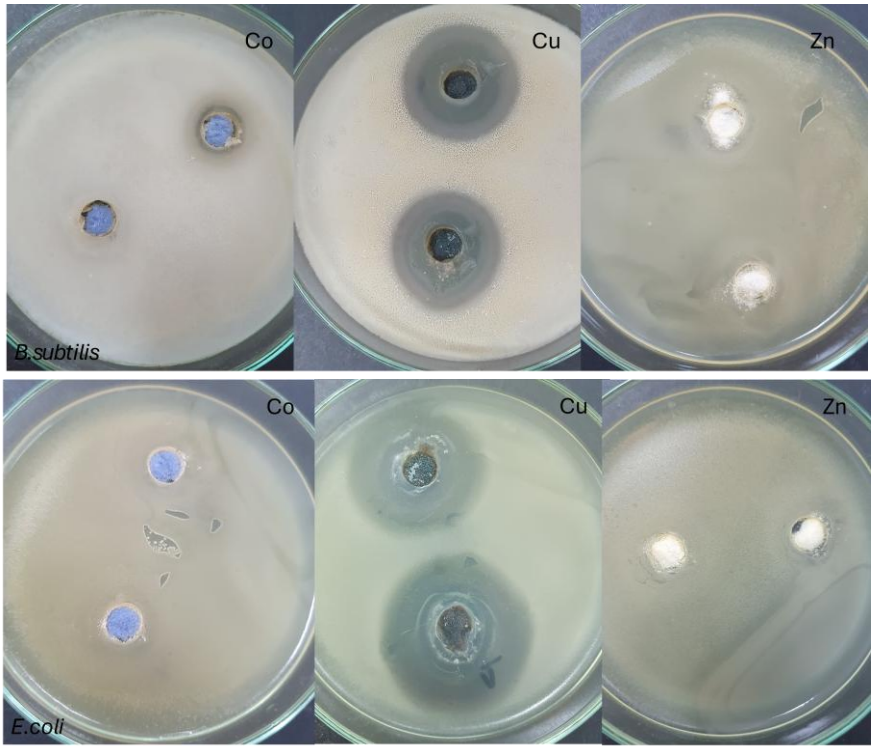

Fig. 8. Variation in antimicrobial activity of substituted bioglasses against *Bacillus subtilis* and *Escherichia coli* for BGCo, BGCu and BGZn.

Overall, BG-Cu exhibited the strongest antimicrobial activity against both bacterial strains, underlining the role of copper in enhancing antibacterial properties. Studies have shown that copper coatings exhibit a strong antibacterial effect by disrupting bacterial membranes, generating reactive oxygen species, and interfering with essential enzymatic functions, leading to cell death [33, 34]. Additionally, copper-doped bioactive materials have demonstrated a metal concentration-dependent antibacterial effect, effectively inhibiting bacterial

growth and biofilm formation [34]. Interestingly, despite the increased protective barrier of Gram-negative bacteria, *E. coli* was found to be more susceptible to bioglass samples than *B. subtilis*, regardless of the metallic ion substitution. This suggests that beyond the bacterial cell wall structure, other factors such as ion release dynamics and surface interactions may play a crucial role in determining antimicrobial efficacy [33, 34].

This preliminary evaluation represents the initial phase of investigating the antimicrobial properties of the bioglasses synthesized in this study. While promising results have been obtained, further research is necessary to validate these findings and explore the mechanisms underlying the observed differences in terms of antibacterial activity. Future work will include testing the antimicrobial activity of bioglass thin films to compare their performance with that of the powders and assess their potential for clinical applications.

These findings underline the versatility of substituted bioglasses in tailoring structural and chemical properties for specific biomedical applications, with copper and zinc showing the most significant effects on particle growth and morphological evolution, while cobalt primarily influences densification and filament-like structures. Since EDX confirmed the presence of substituent elements in all compositions, further studies including elemental mapping are needed to fully assess their spatial distribution within the bioglass matrix.

4. Conclusions

Co-, Cu-, and Zn-substituted bioglasses were successfully synthesized via the sol-gel method, confirming the feasibility of obtaining glassy powders suitable for biomedical applications. The XRD patterns confirmed the amorphous nature of the bioglasses, with minimal crystallization tendencies observed for the substituted samples. The FTIR spectra provided insights into the structural evolution of the bioglass powders, highlighting the elimination of impurities and glass network stabilization through calcination. SEM images illustrated substituent-induced morphological changes, with Co-incorporating samples displaying densified structures and filamentous formations, while Cu-containing bioglass exhibited quasi-spherical particles and increased porosity. EDX spectra confirmed the incorporation of substituting elements (Co, Cu, Zn) into the bioglass matrices. The preliminary antimicrobial tests demonstrated significant activity for Cu-substituted bioglass against both *Bacillus subtilis* and *Escherichia coli*, with inhibition zones exceeding 10 mm for both strains. Zinc-containing bioglass showed moderate activity, particularly against *B. subtilis*, while Co-incorporating sample exhibited limited antimicrobial performance. These findings align with prior reports emphasizing the antibacterial and bioactive properties of modified bioglasses, supporting their suitability for biomedical applications.

Overall, the study highlights the versatility of Co-, Cu-, and Zn-substituted bioglasses in enhancing osteointegration and providing antimicrobial efficacy, as well as their potential for broader biomedical applications, such as combating bacterial infections and promoting tissue repair. Future work will focus on evaluating the properties of thin films derived from these bioglasses and comparing their performance with that of the powder samples.

Acknowledgement

The authors are grateful to the Romanian Government for providing access to the research infrastructure of the National Centre for Micro and Nanomaterials through the National Program titled "Installations and Strategic Objectives of National Interest".

R E F E R E N C E S

[1] J. Huang, "Design and Development of Ceramics and Glasses" (Chapter 20), in Biology and Engineering of Stem Cell Niches, 2017, pp. 315–329.
[2] R. A. Puiu, D. A. Florea, A.-C. Burdușel, et al., "Metallic nanoparticles and metal oxide used in biomedical applications", U.P.B. Sci. Bull., Series B, vol. 85, no. 4, 2023, pp. 113–132.
[3] S. Kumar, P. Mishra, and R. Sharma, "Bioactive Glass—An Extensive Study of the Preparation and Applications of Bioactive Glass Coatings in the Biomedical Field," Coatings, vol. 13, 2023, pp. 112–125.
[4] M. Chen, Y. Wang, P. Yuan, et al., "Multifunctional bioactive glass nanoparticles: Surface-interface decoration and biomedical applications," Regenerative Biomaterials, vol. 11, 2024, pp. 1–15.
[5] P. Zhou, B. L. Garcia, and G. A. Kotsakis, "Comparison of Antibacterial and Antibiofilm Activity of Bioactive Glass Compounds S53P4 and 45S5," BMC Microbiology, vol. 22, 2022, p. 212.
[6] A. Trishala and C. A. Jacob, "The Anti-Bacterial Activity of Bioactive Glass," International Journal of Advanced Research, vol. 4, no. 5, 2016, pp. 1070–1077.
[7] A. A. Mostafa, M. M. H. El-Sayed, A. N. Emam, et al., "Bioactive Glass Doped with Noble Metal Nanoparticles for Bone Regeneration: In Vitro Kinetics and Proliferative Impact on Human Bone Cell Line," RSC Advances, vol. 11, 2021, pp. 25628–25638.
[8] R. Lavric, C. Vreme, C. Busuioc, G.-O. Isopencu, A.-I. Nicoara, O.-C. Oprea, D.-D. Banciu, I. Constantinoiu, and A.-M.-R. Musat, "The Effect of Silver and Samarium on the Properties of Bioglass Coatings Produced by Pulsed Laser Deposition and Spin Coating," Journal of Functional Biomaterials, vol. 14, 2023, p. 560.
[9] X. Li, L. Zhang, and Y. Wang, "Antibacterial Properties and Mechanisms of Gold–Silver Nanocages," Nanoscale, vol. 15, 2023, pp. 345–359.
[10] T. Yamada and S. Takahashi, "Nanostructured Ag-Bioglass Implant Coatings with Antibacterial and Osteogenic Activities," Advanced Materials Interfaces, vol. 10, no. 2, 2023, pp. 1032–1042.
[11] J. N. Oliver, Y. Su, X. Lu, et al., "Bioactive Glass Coatings on Metallic Implants for Biomedical Applications," Bioactive Materials, vol. 4, 2019, pp. 261–270.
[12] C. Berbecaru, H. V. Alexandru, A. Ianculescu, et al., "Bioglass Thin Films for Biomimetic Implants," Applied Surface Science, vol. 255, 2009, pp. 5476–5479.

[13] H. V. Korukonda, N. Suresh, S. K. Saranya, et al., "Fabrication and Characterization of an Innovative Silver- and Gadolinium-Doped Bioglass for Bone Regeneration," Materials Science and Engineering C, vol. 123, 2023, pp. 112–125.
[14] M. Mohan Babu, P. V. Rao, R. K. Singh, et al., "ZnO Incorporated High Phosphate Bioactive Glasses for Guided Bone Regeneration Implants: Enhancement of In Vitro Bioactivity and Antibacterial Activity," Journal of Materials Research and Technology, vol. 15, 2021, pp. 633–646.
[15] M.V. Maximov, O.C. Maximov, L. Motelica, D. Ficai, O.C. Oprea, R.D. Truscă, L.-R. Balahura, R. Pericleanu, A.S. Dumbravă, V.M. Corbu, et al., "Comprehensive Evaluation of 45S5 Bioactive Glass Doped with Samarium: From Synthesis and Physical Properties to Biocompatibility and Antimicrobial Activity," Coatings, vol. 15, 2025, p. 404.
[16] Z. Neščáková, K. Zheng, L. Liverani, et al., "Multifunctional Zinc Ion Doped Sol–Gel Derived Mesoporous Bioactive Glass Nanoparticles for Biomedical Applications," Acta Biomaterialia, vol. 114, 2020, pp. 68–82.
[17] I. Hammami, S. R. Gavinho, S. K. Jakka, et al., "Antibacterial Biomaterial Based on Bioglass Modified with Copper for Implants Coating," Journal of Functional Biomaterials, vol. 14, no. 7, 2023, p. 369.
[18] H. Ture, "Development of Copper-Doped Bioglass/Alginate Composite Membranes: Preliminary Results on Their Characterization and Antimicrobial Properties," Materials Today Communications, vol. 21, 2019, p. 100583.
[19] F. Baino, M. Montazerian, and E. Verné, "Cobalt-Doped Bioactive Glasses for Biomedical Applications: A Review," Materials, vol. 16, 2023, p. 4994.
[20] T. T. Tran, N. B. Nichita, M.-O. Dobrica, et al., "In vitro biocompatibility investigation of silver and zinc modified hydroxyapatite deposited on implant materials", U.P.B. Sci. Bull., Series B, vol. 82, no. 3, 2020, pp. 233–248.
[21] A. E. Stoica (Oprea), A. C. Bîrcă, M. L. Pițigoi (Pandel), et al., "Nanostructured zinc oxide for wound dressings", U.P.B. Sci. Bull., Series B, vol. 86, no. 2, 2024, pp. 161–172.
[22] A. K. Solanki, F. V. Lali, H. Autefage, et al., "Bioactive Glasses and Electrospun Composites That Release Cobalt to Stimulate the HIF Pathway for Wound Healing Applications," Materials Today Bio, vol. 16, 2023, p. 100452.
[23] A.-L. Mîrt, D. Ficai, O.-C. Oprea, G. Vasilievici, and A. Ficai, "Current and Future Perspectives of Bioactive Glasses as Injectable Material," Nanomaterials, vol. 14, 2024, p. 1196.
[24] J. M. Smith, R. A. Martin, G. J. Cuello, and R. J. Newport, "Structural characterisation of hypoxia-mimicking bioactive glasses," J. Mater. Chem. B, vol. 1, no. 12, pp. 1296–1303, 2013.
[25] S. Kumar, A. Patel, K. Desai, et al., "Synthesis and Characterization of ZnO(MgO)-CaO-SiO_2-P_2O_5 Bioglass Obtained by Sol-Gel Method for Biomedical Applications," Biomaterials Science, vol. 11, 2023, pp. 456–468.
[26] A. C. Bîrcă, A. E. Stoica, F. Iordache, et al., "ZnO thin films by pulsed laser deposition with applications in sensors", U.P.B. Sci. Bull., Series B, vol. 86, no. 2, 2024, pp. 147–160.
[27] I. Constantin, P. Moldovan, "Microstructure and corrosion resistance of electrodeposited Zn-Ni-P thin films", U.P.B. Sci. Bull., Series B, vol. 78, no. 1, 2016, pp. 185–192.
[28] C. R. Dumitrescu, I. A. Neacsu, V. A. Surdu, et al., "Maturation of hydroxyapatite from biogenic calcium source – A comparative study", U.P.B. Sci. Bull., Series B, vol. 84, no. 1, 2022, pp. 21–28.
[29] F. G. Mecca, D. Bellucci, and V. Cannillo, "Effect of Thermal Treatments and Ion Substitution on Sintering and Crystallization of Bioactive Glasses: A Review," Materials, vol. 16, no. 4651, 2023.

[30] D. Ghezzi, E. Sassoni, M. Boi, M. Montesissa, N. Baldini, G. Graziani, and M. Cappelletti, "Atomic force microscopic investigations of transient early-stage bacterial adhesion and antibacterial activity of silver and ceria modified bioactive glass," Antibiotics, vol. 12, 2023, p. 55.
[31] D. U. Tulyaganov, S. Agathopoulos, P. Valério, and J. M. Ferreira, "Classical Bioglass® and innovative CaO-rich bioglass powders processed by Spark Plasma Sintering: A comparative study," J. Eur. Ceram. Soc., vol. 31, no. 14, pp. 2589–2598, 2011.
[32] J. Patel, S. Thakur, and L. Zhang, "Optimization of Silver-Containing Bioglass Nanoparticles Envisaging Biomedical Applications," J. Mater. Chem. B, vol. 11, 2023, pp. 987–1001.
[33] A. L. Oliveira, M. V. Pereira, J. P. Oliveira, et al., "Influence of Copper-Strontium Co-Doping on Bioactivity and Antibacterial Properties of Sol-Gel Derived Bioactive Glasses," J. Non-Cryst. Solids, vol. 604, 2023, p. 121871.
[34] D. Ghezzi, E. Sassoni, M. Boi, et al., "Antibacterial and Antibiofilm Activity of Nanostructured Copper Films Prepared by Ionized Jet Deposition," Antibiotics, vol. 12, 2023, p. 55.